

# Octagraphene as a Versatile Carbon Atomic Sheet for Novel Nanotubes, Unconventional Fullerenes and Hydrogen Storage

Xian-Lei Sheng,<sup>1</sup> Hui-Juan Cui,<sup>1</sup> Fei Ye,<sup>2</sup> Qing-Bo Yan,<sup>2</sup> Qing-Rong Zheng<sup>1</sup> and Gang Su<sup>1a</sup>

<sup>1</sup>*Theoretical Condensed Matter Physics and Computational  
Materials Physics Laboratory, College of Physical Sciences,  
Graduate University of Chinese Academy of Sciences, Beijing 100049, China*

<sup>2</sup>*College of Materials Science and Opto-Electronic Technology,  
Graduate University of Chinese Academy of Sciences, Beijing 100049, China*

## Abstract

We study a versatile structurally favorable periodic  $sp^2$ -bonded carbon atomic planar sheet with  $C_{4v}$  symmetry by means of the first-principles calculations. This carbon allotrope is composed of carbon octagons and squares with two bond lengths and is thus dubbed as octagraphene. It is a semimetal with the Fermi surface consisting of one hole and one electron pocket, whose low-energy physics can be well described by a tight-binding model of  $\pi$ -electrons. Its Young's modulus, breaking strength and Poisson's ratio are obtained to be 306  $N/m$ , 34.4  $N/m$  and 0.13, respectively, which are close to those of graphene. The novel sawtooth and armchair carbon nanotubes as well as unconventional fullerenes can also be constructed from octagraphene. It is found that the Ti-absorbed octagraphene can be allowed for hydrogen storage with capacity around 7.76 wt%.

PACS numbers: 61.46.-w, 62.25.-g, 73.22.-f, 61.48.De

---

<sup>a</sup> Corresponding author. E-mail: gsu@gucas.ac.cn

## I. INTRODUCTION

The discovery of graphene [1] opens a new era of fundamental research and technological applications of carbon-based materials. Graphene is an elegant two-dimensional (2D) material exhibiting exceptional electrical, thermal, mechanical and optical properties, and its low-energy behavior of electrons is described by a (2+1)-dimensional relativistic quantum theory [2–4]. Stimulated by the tremendous interest of graphene, a great number of novel carbon structures were proposed and investigated in the past years (e.g. Refs. [5–10]). Among others, two intriguing  $sp$ - $sp^2$ -bonded monolayers of elemental carbon, graphyne [11] and graphdiyne [12, 13], and an insulating 2D hydrocarbon layer, graphane [14, 15], are typical examples, all of which were experimentally obtained. It appears that there is a growingly extensive interest to seek for more 2D allotropes of carbon with amazing physical and chemical properties as well as possibly diverse applications.

Graphene has a perfect honeycomb lattice with  $C_{6v}$  symmetry. Recent studies [6, 16, 17] show that the line defects with octagons and pentagons could be formed self-assembly in graphene. The formation of small carbon molecules with various polygon rings has also been studied from experimental aspects [18]. Inspired by these observations, we propose a stable 2D periodic atomic sheet consisting of carbon octagons, coined as *octagraphene*, which possesses intriguing properties and might be synthesized experimentally by line defects or acetylene scaffolding ways. As shown in Fig. 1(a), octagraphene comprises of carbon octagons and squares with two bond lengths that forms a square lattice with  $C_{4v}$  symmetry. By means of the first-principles calculations, it is shown that octagraphene is energetically and kinetically stable, and is more favorable in energy than graphyne and graphdiyne, although it is metastable against graphene. By rolling octagraphene along specific directions, we can get novel sawtooth and armchair carbon nanotubes [Fig. 1(b)] that are metallic, which can escape from the difficult separation of usual metallic and semiconducting carbon nanotubes [19]; by wrapping octagraphene and making use of pentagons, hexagons or heptagons as caps, many stable unconventional fullerenes such as  $C_{36}$ ,  $C_{48}$ ,  $C_{80}$ ,  $C_{96}$  and so forth [Fig. 1(c)] can be constructed. The electronic properties of octagraphene manifest that it is a semimetal with small density of states (DOS) around the Fermi level, whose Fermi surface consists of one hole and one electron pockets centered at  $\Gamma$  and  $M$  points, respectively. The low-energy physics of octagraphene can be well described by a tight-binding model of  $\pi$  electrons. Octagraphene has the density of  $0.68 \text{ mg/m}^2$ , Young's modulus of  $306 \text{ N/m}$ , breaking strength of  $34.4 \text{ N/m}$  and

Poisson's ratio of 0.13. It could be the strongest periodic carbon sheet after graphene till now. An energy gap can be opened by doping boron nitrogen pairs. The possible routes for obtaining octagraphene are suggested. The Ti-absorbed octagraphene can also be used for hydrogen storage with capacity of 7.76 wt%. With these amazing characters, we anticipate that octagraphene, similar to its cousin—graphene, once being obtained, will likewise have a crucial impact in physics, chemistry, materials and information sciences.

The rest of this article is organized as follows. In Sec. II, the calculational methods are described. In Sec. III, the geometrical structure, mechanical properties, electronic structures and low-energy physics of octagraphene are presented. In Sec. IV, new carbon nanotubes and unconventional fullerenes from octagraphene are given. The band engineering and hydrogen storage of octagraphene are discussed in Sec. V. Finally, a conclusion is briefly presented.

## II. CALCULATIONAL METHODS

Both the first-principles calculations within the framework of the density-functional theory (DFT) [20, 21] and the tight-binding approximation (TBA) [22] are invoked to study this 2D system. For the first-principles method, primary calculations were performed within the Vienna *ab initio* simulation package (VASP) [23, 24] with the projector augmented wave (PAW) method [25]. Both the local density approximation (LDA) in the form of Perdew-Zunger [26] and generalized gradient approximation (GGA) developed by Perdew and Wang [27] were adopted for the exchange correlation potentials. The plane-wave cutoff energy is taken as 400 eV. The Monkhorst-Pack scheme for k-point samplings with  $32 \times 32 \times 1$  mesh for planar sheets and  $1 \times 1 \times 100$  mesh for nanotubes were used to sample the Brillouin zone [28]. The supercells are used for calculations of isolated sheet structures, and the distance between two layers is about 10 Å to avoid interactions. The geometries were optimized when the remanent Hellmann-Feynman forces on the ions are less than 0.01 eV/Å. Phonon calculations with a k-mesh of  $8 \times 8 \times 1$  are performed using the density functional perturbation theory [29].

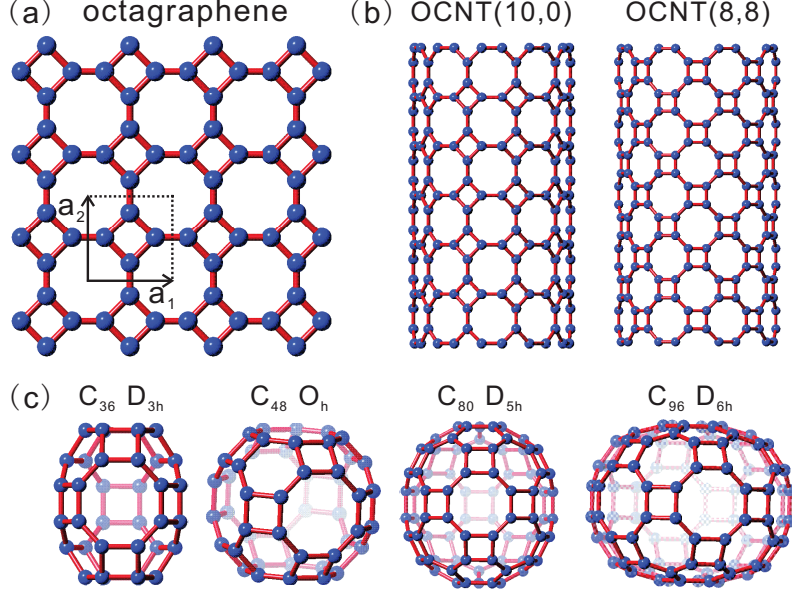


FIG. 1. (Color online) Schematic depiction of the structures of (a) octagraphene, where a unit cell is indicated with the unit vectors  $\mathbf{a}_1$  and  $\mathbf{a}_2$ ; (b) single-wall sawtooth (10,0) and armchair (8,8) carbon nanotubes rolled from octagraphene; and (c) unconventional fullerenes of  $C_{36}$ ,  $C_{48}$ ,  $C_{80}$  and  $C_{96}$  obtained from octagraphene.

### III. OCTAGRAPHENE

#### A. Geometrical structure and mechanical properties

The optimized geometric structure of octagraphene is presented in Fig. 1(a). Carbon atoms in octagraphene form a square lattice with the lattice constant  $a_0 = 3.45 \text{ \AA}$ , where a unit cell contains four carbon atoms. Similar to graphene, every carbon atom in octagraphene has three  $sp^2$ -bonded nearest neighbors, forming three  $\sigma$  bonds. In addition, octagraphene has two types of bond lengths,  $1.48 \text{ \AA}$  of intra-squares and  $1.35 \text{ \AA}$  of inter-squares, and two bond angles  $90^\circ$  and  $135^\circ$ .

The cohesive energy  $E_c$  per atom as a function of lattice constant ( $a/a_0$ ) is given in Fig. 2(a) for graphene, octagraphene, graphyne and graphdiyne, respectively. It is clear that a single minimum of  $-E_c$  appears at  $a/a_0 = 1$  for these 2D structures, suggesting that they are energetically stable. Note that the minimum of  $-E_c$  for octagraphene is smaller than those of graphyne and graphdiyne but larger than that of graphene, suggesting octagraphene is more energetically stable than graphyne and graphdiyne but metastable against graphene. Fig. 2(b) gives the phonon

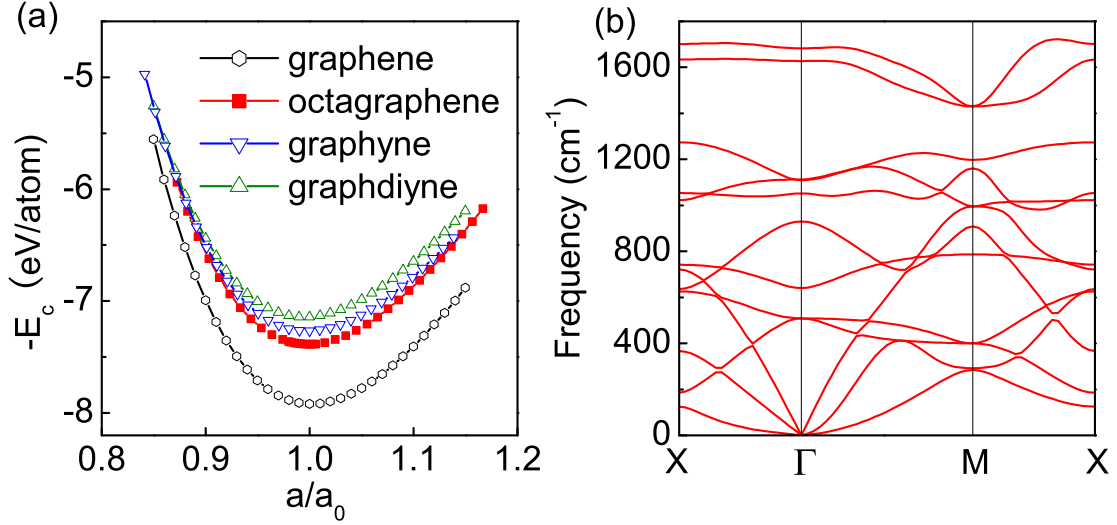


FIG. 2. (Color online) (a) Cohesive energy per atom as a function of lattice constant  $a$  for graphene, octagraphene, graphyne and graphdiyne, respectively, where  $a_0$  is the optimized lattice constant. (b) Phonon spectra of octagraphene.

spectra of octagraphene. No imaginary phonon modes are found, implying that octagraphene is also kinetically stable. We performed quantum molecular dynamics simulations and found that at temperature 500 K the planar structure of octagraphene still maintains. Considering that graphyne and graphdiyne were already obtained experimentally, it is reasonable to believe that octagraphene can be synthesized in lab or likely already exists in Nature. In fact, carbon rings with four or eight sides have already been observed in some experiments [16, 17].

For a comparison, the cohesive energy  $E_c$ , density  $\rho$ , bond length  $l_{CC}$ , energy gap  $E_g$ , Young's modulus  $E$ , breaking strength  $\sigma$  and Poisson's ratio  $\nu$  for graphene, octagraphene, graphyne and graphdiyne, respectively, are collected in Table I. Notice that apart from the experimental data of graphene taken from literature, all data presented here were calculated by ourselves using the same method. As octagons in octagraphene are larger in size than hexagons in graphene, octagraphene has the density ( $0.68 \text{ mg/m}^2$ ) slightly smaller than that of graphene ( $0.77 \text{ mg/m}^2$ ).

Now let us discuss the mechanical properties of octagraphene. As it has a  $C_{4v}$  symmetry, only three elastic constants  $c_{ij}$  are independent. Our DFT calculations estimate that the values of  $c_{11}$ ,  $c_{12}$  and  $c_{44}$  of octagraphene are 296, 46, and 49  $\text{N/m}$ , respectively. The Young's modulus  $E$

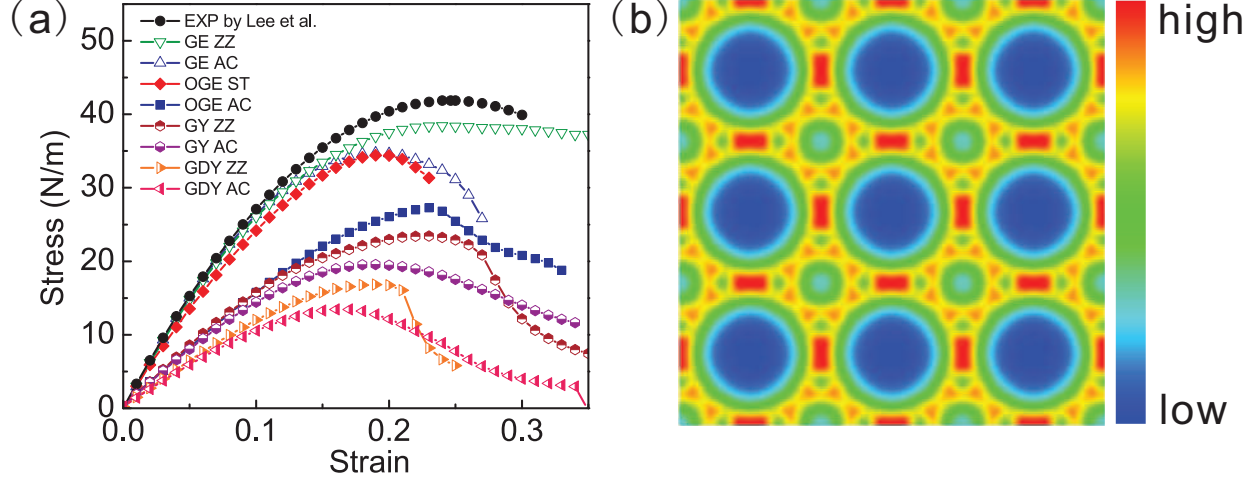


FIG. 3. (Color online) (a) Stress-strain curves of graphene (GE), octagraphene (OGE), graphyne (GY) and graphdiyne (GDY) along armchair (AC) and zigzag (ZZ) or sawtooth (ST) directions. The experimental data of graphene are taken from [30]. (b) Valence electron density of octagraphene.

of octagraphene is obtained to be 306 and 168  $N/m$  along the sawtooth and armchair directions (see below), respectively, in comparison to those of graphene 350  $N/m$ , graphyne 245  $N/m$  and graphdiyne 174  $N/m$ . The stress-strain curves for graphene, octagraphene, graphyne and graphdiyne under a uniaxial tension along two non-chiral directions are illustrated in Fig. 3(a). The ultimate tensile strength or the breaking strength  $\sigma$  of octagraphene is 34.4 and 27.3  $N/m$  along the sawtooth and armchair directions, respectively, which are quite comparable with those of graphene 38.4  $N/m$  (zigzag direction) and 34.8  $N/m$  (armchair direction) but larger than those of graphyne (23.4 and 19.5  $N/m$ ) and graphdiyne (16.8, 13.4  $N/m$ ). The experimental values [30] of  $E$  and  $\sigma$  for graphene are  $340 \pm 50$   $N/m$  and  $42 \pm 4$   $N/m$ , respectively, showing that our DFT calculations are quite reliable. The Poisson's ratio of octagraphene is 0.13 (sawtooth direction) and 0.47 (armchair direction), which are comparable with 0.21 (zigzag direction) and 0.17 (armchair direction) of graphene. The Poisson's ratio of graphyne and graphdiyne can be found in Table I. From above results we see that octagraphene has the mechanical properties very similar to graphene, and might be the strongest carbon atomic sheet after graphene till now.

## B. Electronic structures

The valence electron density, electronic structures and the DOS of octagraphene are obtained by means of the DFT and TBA calculations, respectively. From Fig. 3(b) one may see that more

TABLE I. The symmetry, lattice constant ( $a_0$ ), bond lengths  $l_{CC}$ , plane density  $\rho$ , cohesive energy ( $E_c$ ), energy gap  $E_g$  between the bottom of conduction band and the top of valence band, Young's modulus  $E$ , breaking strength  $\sigma$  and Poission's ratio  $\nu$  for graphene, octagraphene, graphyne and graphdiyne, respectively.

Structure	method	symmetry	$a_0$ (Å)	$l_{CC}$ (Å)	$\rho$ (mg/m <sup>2</sup> )	$E_c$ (eV/atom)	$E_g$ (eV)	$E$ (N/m)	$\sigma$ (N/m)	$\nu$
graphene	GGA	$C_{6v}$	2.46	1.42	0.77	7.92	0	350	38.4,34.8	0.21,0.17
graphene	Exp.[1, 30–33]	$C_{6v}$	2.458	1.419	0.77	7.37	0	340±50	42±4	0.165
octagraphene	GGA	$C_{4v}$	3.45	1.48,1.35	0.68	7.39	-4.03	306,168	34.4,27.3	0.13,0.47
graphyne	GGA	$C_{6v}$	6.88	1.22,1.42	0.59	7.26	0.48	245	23.4,19.5	0.38,0.41
graphdiyne	GGA	$C_{6v}$	9.45	1.23,1.43	0.47	7.14	0.51	174	16.8,13.4	0.41,0.44

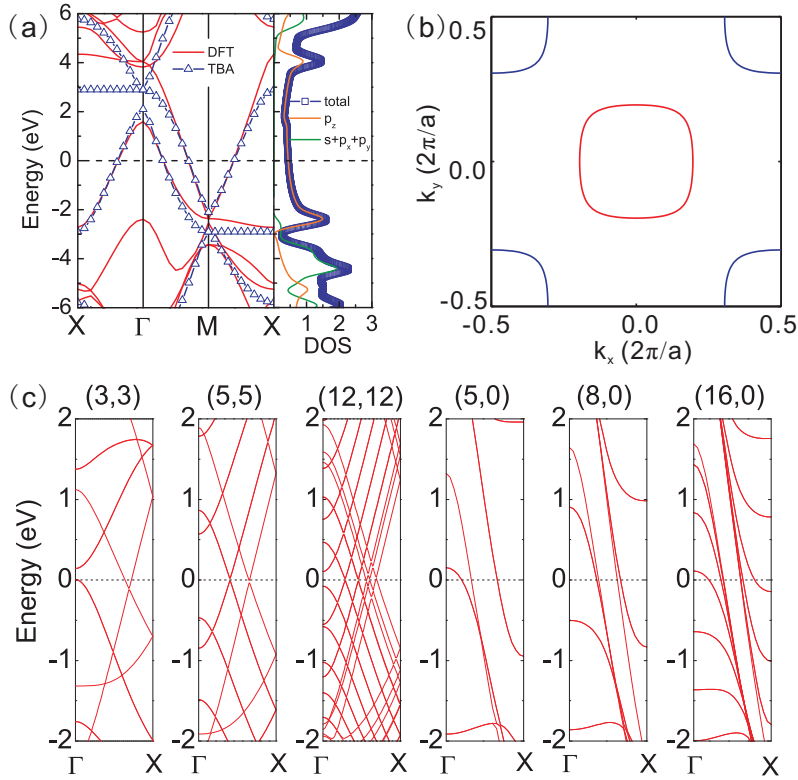


FIG. 4. (Color online) (a) Electronic band structures and density of states (DOS) of octagraphene calculated by the density functional theory (DFT) and the tight-binding approximation (TBA) methods. (b) Fermi surface of octagraphene, where the hole packet (red) is at  $\Gamma$  point, and the electron pocket (blue) is at  $M$  point. (c) Energy bands of octagraphene nanotubes (3,3), (5,5), (12,12), (5,0), (8,0) and (16,0).

electrons are distributed on the inter-square bonds than on the intra-square bonds in octagraphene, which is well consistent with its structural feature, showing an unequal  $sp^2$  hybridizing character. The electronic structures in Fig. 4(a) show that octagraphene is a semimetal, as its top of valence band and the bottom of conduction band are located at  $\Gamma$  and  $M$  points in the Brillouin zone, respectively, giving rise to an indirect *negative* band gap (-4.03 eV), and leading to the Fermi level passes through both the conduction and valence bands. Thus, in contrast to graphene, the charge carriers in octagraphene have both holes and electrons around the Fermi level. Note that graphene is also a semimetal or a zero-gap semiconductor because its valence and conduction bands touch at  $K$  points, while graphyne and graphdiyne are semiconductors with narrow band gap of 0.48 and 0.51 eV, respectively.

The projected DOS of octagraphene shows that the energy bands near the Fermi surface are predominantly contributed by the  $2p_z$  orbital of carbon atom, forming the same  $\pi$ -bond as that in graphene. The Fermi surface of octagraphene is plotted in Fig. 4(b), which consists of a hole pocket at  $\Gamma$  point and an electron pocket at  $M$  point. Since each unit cell contributes four electrons with two bonding states and two antibonding states, each point in the Brillouin zone should be filled with  $2 \times 2$  electrons, and the number of unoccupied states in valence band is just equal to that of occupied states in conduction band, resulting in that the hole and electron pockets share the same area.

### C. Low-energy physics

To describe the low-energy physics near the Fermi surface of octagraphene, we propose a tight-binding model which contains only  $\pi$  electrons with nearest neighbor hoppings. The Hamiltonian can be written as

$$H = t \sum_{\langle i,j \rangle, \sigma} (\hat{c}_{i,\sigma}^\dagger \hat{c}_{j,\sigma} + h.c.) + t' \sum_{\langle\langle i,j \rangle\rangle, \sigma} (\hat{c}_{i,\sigma}^\dagger \hat{c}_{j,\sigma} + h.c.), \quad (1)$$

where  $\hat{c}_{i,\sigma}$  and  $\hat{c}_{i,\sigma}^\dagger$  are the electron annihilation and creation operators at site  $i$  with spin  $\sigma$ ,  $\langle i, j \rangle$  runs over the nearest neighbors within the same square and  $t$  is the corresponding hopping amplitude of electrons,  $\langle\langle i, j \rangle\rangle$  runs over the nearest neighbors connecting different squares and  $t'$  is



the corresponding hopping amplitude. In the matrix form, the Hamiltonian reads

$$H_{\mathbf{k}} = \begin{pmatrix} 0 & t & t'e^{-ik_y} & t \\ t & 0 & t & t'e^{ik_x} \\ t'e^{ik_y} & t & 0 & t \\ t & t'e^{-ik_x} & t & 0 \end{pmatrix}, \quad (2)$$

where  $k_x$  and  $k_y$  are  $x$  and  $y$  components of momentum of  $\pi$  electrons, and the lattice spacing  $a_0 = 1$  is taken. The dispersion  $E(\mathbf{k})$  of octagraphene within the TBA is determined by

$$E(\mathbf{k})^4 - 2(t'^2 + 2t^2)E(\mathbf{k})^2 + 4t't^2(\cos k_x + \cos k_y)E(\mathbf{k}) + t'^2[t'^2 - 4t^2(\cos k_x + \cos k_y)] = 0. \quad (3)$$

The TBA results are in good agreement with those obtained by the DFT calculations [Fig. 4(a)], implying that the low-energy properties of  $\pi$  electrons in octagraphene can be well described by the TBA Hamiltonian, where the fittings give  $t = -2.5$  eV and  $t' = -2.9$  eV. For graphene,  $t = -2.7$  eV [34].

#### D. Fabricating suggestions

To obtain the structure of octagraphene experimentally, we suggest that one may make the line defects periodically in graphene, and then connect properly the broken bonds of carbon atoms, as demonstrated in Fig. 5. In addition, it may be possible to synthesize it through the acetylene scaffolding ways [10, 18].

## IV. OCTAGRAPHENE NANOTUBES AND FULLERENES

By rolling octagraphene, the novel single-walled carbon nanotubes can also be obtained. For this purpose, let us define the chiral vector  $\vec{C}_h$  of octagraphene carbon nanotube (OCNT) by  $\vec{C}_h = n\vec{a}_1 + m\vec{a}_2 \equiv (n, m)$ , where  $n$  and  $m$  are integers with  $0 \leq |m| \leq n$  because of the  $C_{4v}$  symmetry. We call  $(n, 0)$  the sawtooth OCNT ( $m = 0$ ,  $\theta = 0^\circ$ ), and  $(n, n)$  the armchair OCNT ( $m = n$ ,  $\theta = 45^\circ$ ), where the chiral angle is defined as  $\cos \theta = n/\sqrt{n^2 + m^2}$ . The tube diameter is given by  $d_t = |\vec{C}_h|/\pi = a_0\sqrt{n^2 + m^2}/\pi$ . The geometric structures of sawtooth OCNT (10,0) and armchair OCNT (8,8) are presented in Fig. 1(b) as examples, whose structural stabilities were verified by the DFT calculations. The energy bands of OCNT (3,3), (5,5), (12,12), (5,0), (8,0) and (16,0) are

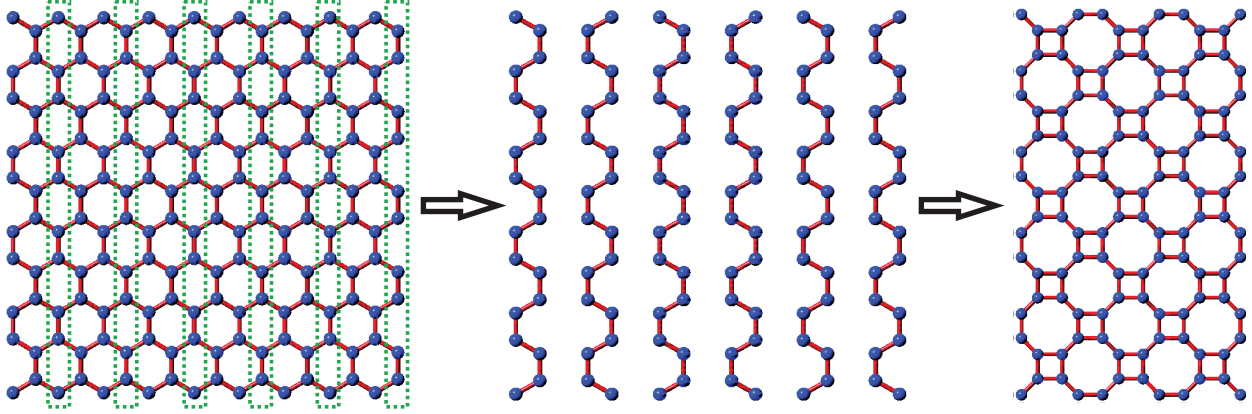


FIG. 5. (Color online) A schematic demonstration how to utilize the line defects in graphene to obtain octagraphene.

given in Fig. 4(c), which show that regardless of the curvature effect, the single-walled OCNTs, either sawtooth or armchair, are all metallic.

In addition, by wrapping octagraphene and using pentagons, hexagons or heptagons as caps, many structurally stable unconventional carbon fullerenes can be built. The optimized examples like  $C_{36}$ ,  $C_{48}$ ,  $C_{80}$  and  $C_{96}$  are shown in Fig. 1(c). These results show that octagraphene is indeed a versatile 2D crystalline allotrope of carbon after graphene.

## V. BAND ENGINEERING AND HYDROGEN STORAGE

### A. Boron nitrogen pair doping

Similar to graphene and carbon nanotubes[35, 36], the semimetallic octagraphene may be applicable in the band engineering via the chemical doping. In fact our calculation reveals that a band gap opens if the octagraphene is substitutionally doped with boron and nitrogen (B-N) pairs, as shown in Fig. 6, where eleven structures for different doping configurations and a pure B-N octa-square structure are considered. All these doped structures are energetically favorable. In Fig. 6 (a), the structures of number 1-11 are those of octagraphene of  $4 \times 4$  supercell with substituting carbon (blue ball) by boron (red ball) and nitrogen (green ball) atom pairs, and the structure of number 12 is the pure B-N octagon-square structure of  $3 \times 3$  supercell. In the first structure two carbon neighbors are replaced by one B-N pair; in the second (third) structure a square (octagon) is substituted by two (four) B-N pairs; in the fourth (sixth, seventh or ninth) one a nanoribbon in

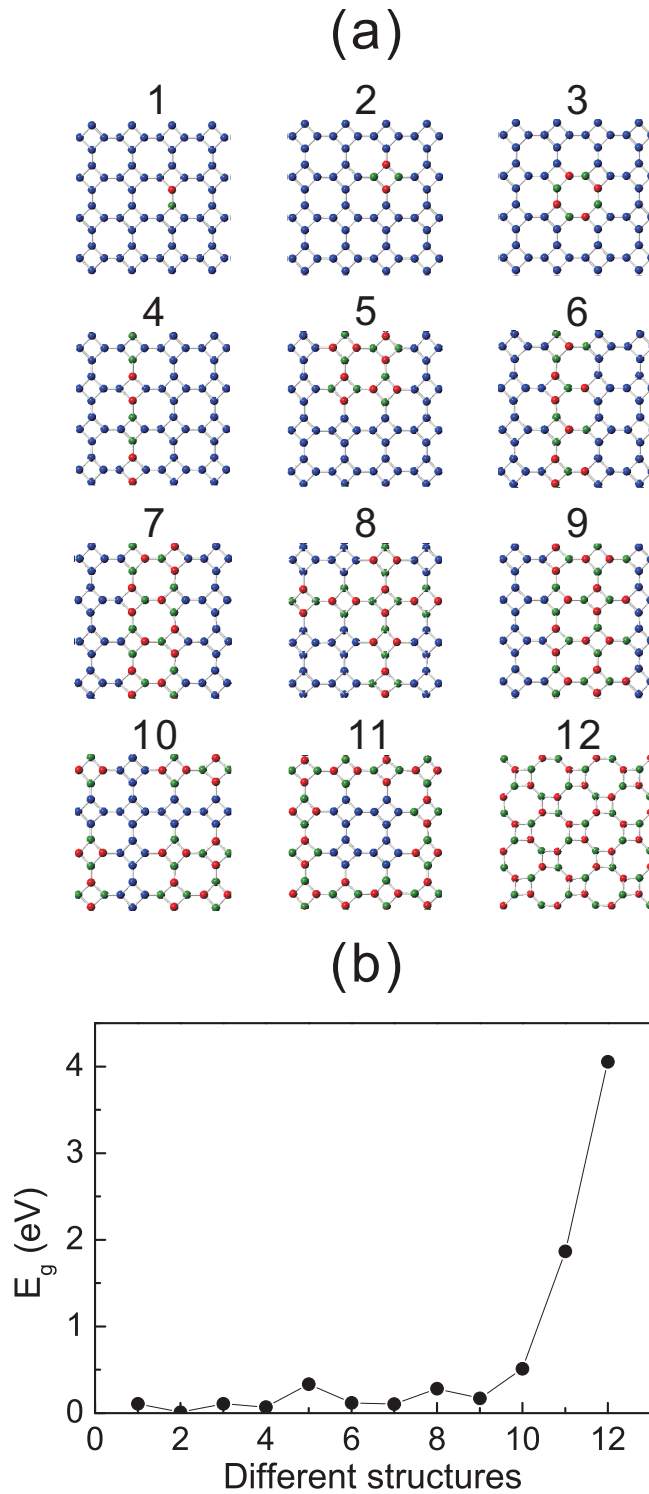


FIG. 6. (a) Schematic structures of boron nitrogen pairs substitutionally doped octagraphene with different doping configurations, where carbon, boron, and nitrogen atoms are colored in blue, red, and green, respectively. (b) The corresponding band gaps ( $E_g$ ) for different structures of (a), where the doping concentration is from small to large in sequence.

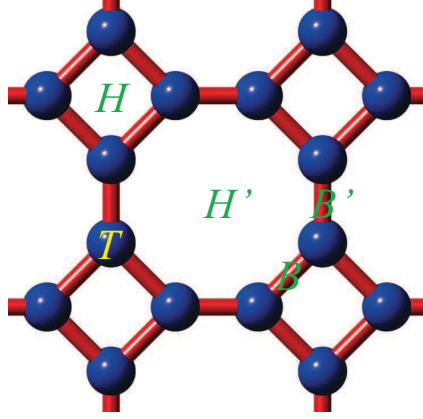


FIG. 7. (Color online) There are five possible adsorption sites of metal atoms on octagraphene, including one top site on C atoms ( $T$ ), two bridge sites on top of intra-square ( $B$ ) and inter-square ( $B'$ ) C-C bond, respectively, and two hollow sites on top of square ( $H$ ) and octagon ( $H'$ ), respectively.

octagraphene is substituted by four (eight, twelve or sixteen) B-N pairs; in the fifth one a  $2 \times 2$  supercell is replaced by eight B-N pairs; in the eighth one a cross is replaced by fourteen B-N pairs; the tenth one is the dual structure of the eighth; the eleventh is the dual structure of the fifth. The band gap varies significantly for different doping configurations, as shown in Fig. 6 (b). It is seen that the boron nitrogen pair doped octagraphene can open a gap from 0.009 eV (structure 2) to 1.866 eV (structure 11), which can gain some insights for nanoelectronics. It is noting that the band gaps of most of structures considered here are around 0.2 eV, even when the doping concentration is as large as 50.82% (structure 9), which is quite different from the doped graphene [37]. Considering that the GGA usually underestimates the band gap, the present doping study gives useful information for the band engineering in octagraphene.

## B. Hydrogen storage

Next, let us consider the possibility of hydrogen storage in octagraphene. In general, there are two ways to realize this purpose. One is that hydrogen atoms can be absorbed on carbons via the chemical bond to form a new hydrocarbon sheet, similar to graphane [14]; the other is that the hydrogen molecules can be adsorbed physically on some metal atoms (e.g. Ti, Ca, Al, etc.) that are deposited on the sheet of octagraphene. In the former case, the hydrogen storage capacity of octagraphene can reach 7.7 wt% as graphane does [14]. In the latter case, the hydrogen capacity depends on the adsorption configuration of metal atoms. There are five possible adsorption

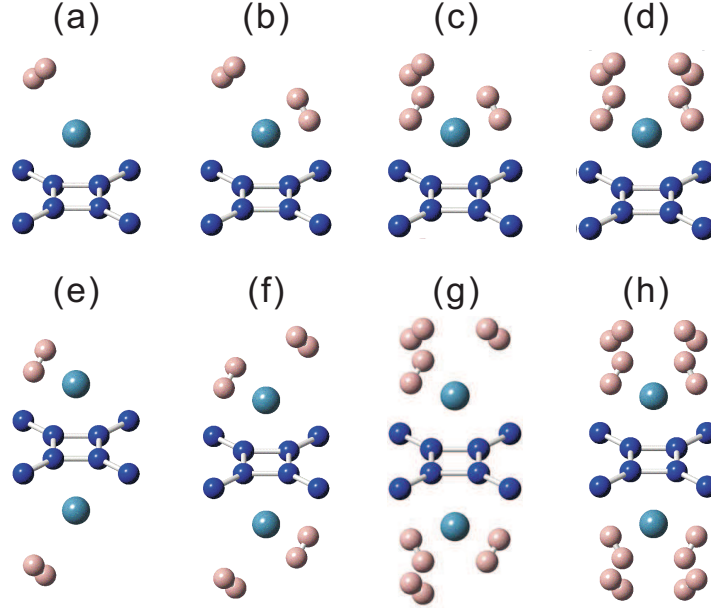


FIG. 8. (Color online) The configuration of four hydrogen molecules adsorbed on each Ti atom at  $H_1$  site. (a)-(d) reveal the single-side hydrogen storage configurations with one, two, three and four hydrogen molecules adsorbed on each Ti atom, respectively; (e)-(h) show the double-side hydrogen storage configurations with one, two, three and four  $H_2$  adsorbed on each Ti atom, respectively; where C, Ti and H atoms are colored in dark blue, bluish green and brick red, respectively.

positions for metal atoms (see Fig. 7), including one top site on C atoms ( $T$ ), two bridge sites on top of intra-square ( $B$ ) and inter-square ( $B'$ ) C-C bond, respectively, and two hollow sites on top of square ( $H$ ) and octagon ( $H'$ ), respectively. To analyze the stability of these five adsorption configurations, we calculate the cohesive energy  $E_{b-M}$  with  $M$  the adsorbed metal atom by

$$E_{b-M} = [E_{octa} + nE_M - E_{M-octa}]/n, \quad (4)$$

where  $E_{octa}$ ,  $E_M$  and  $E_{M-octa}$  are the total energies of pure octagraphene,  $M$  atom and octagraphene with adsorbed metal  $M$ , respectively. For Ti doping ( $M=Ti$ ),  $H$  site is the most stable position with cohesive energy of 2.71 eV per Ti atom.

Figs. 8(a)-(d) present single-side hydrogen storage configurations with one, two, three and four hydrogen molecules adsorbed on each Ti atom. The average adsorption energy per  $H_2$  is 0.207 eV, 0.361 eV, 0.336 eV and 0.325 eV, respectively. Figs. 8 (e)-(h) give double-side hydrogen storage configurations with one, two, three and four  $H_2$  adsorbed on each Ti atom. The average adsorption energy per  $H_2$  is 0.235 eV, 0.355 eV, 0.336 eV and 0.325 eV, respectively. In this case, the hydrogen storage capacity could reach 7.76 wt% for Ti [as shown in Fig. 8(h)], which is very

close to that of Ca-adsorbed graphene, say 8.4 wt% [40]. We also perform the same calculation for Al and Ca atoms ( $M=Al$  or Ca), respectively, and found that the adsorption energy of hydrogen molecule is too small. The adsorption energy of Ti-adsorbed octagraphene is quite promising, say, about 0.3 eV/H<sub>2</sub>. It appears that the hydrogen storage capacity of octagraphene is close to that of fullerenes [38], carbon nanotubes [39] and graphene [40].

## VI. CONCLUSION

In conclusion, we propose a periodic carbon sheet by the first-principles calculations. This novel carbon monolayer is a  $sp^2$ -hybridized structure and coined as octagraphene. Unlike graphene, octagraphene is composed of carbon squares and octagons possessing  $C_{4v}$  symmetry, and is more favorable in energy than graphyne and graphdiyne. Its optimized structure has two bond lengths with 1.48 Å within each square and 1.35 Å between adjacent squares. The band structure shows that it is a semimetal with Fermi surface consisting of one hole pocket and one electron pocket. In order to describe the low-energy physics of octagraphene, we also suggest a tight binding model of  $\pi$  electrons which is uncovered to agree well with DFT calculations, and is quite helpful for further exploring the properties of octagraphene in a magnetic field or emergent quantum phenomena such as quantum Hall effect, Kondo effect, and so on in octagraphene. The intriguing mechanical properties of octagraphene are also obtained, which are observed close to those of graphene. Similar to graphene, we find that octagraphene can also be rolled seamlessly to form stable carbon nanotubes and unconventional fullerenes. By substitutionally doping boron nitrogen pairs, we disclose that the semimetallic octagraphene can be turned into a semiconductor with a band gap, the property will be useful for possible applications in nanoelectronics. This new carbon allotrope has also the possibility for hydrogen storage. Our calculation shows that for the 2D octagraphene sheet the hydrogen storage capacity could reach 7.76% via Ti-adsorption that is close to that of graphene. Finally, we would like to mention that one might obtain this new kind of carbon atomic sheet via making line defects in graphene or through the acetylene scaffolding ways.

## ACKNOWLEDGMENTS

We are grateful to Dr. Eric Germaneau for useful discussions. All calculations were completed in the Shanghai Supercomputer Center, China. This work is supported by the NSFC (Grants No. 90922033, No. 10934008, No. 10974253, No. 10904081 and No. 11004239), the MOST of China (Grant No. 2012CB932900) and the CAS.

- 
- [1] K. S. Novoselov, A. K. Geim, S. V. Morozov, D. Jiang, Y. Zhang, S. V. Dubonos, I. V. Grigorieva and A. A. Firsov, *Science* **306**, 666 (2004).
  - [2] A. Geim, *Science* **324**, 1530 (2009).
  - [3] A. H. Castro Neto, F. Guinea, N. M. R. Peres, K. S. Novoselov and A. K. Geim, *Rev. Mod. Phys.* **81**, 109 (2009).
  - [4] N. M. R. Peres, *Rev. Mod. Phys.* **82**, 109 (2010).
  - [5] Vincent H. Crespi, Lorin X. Benedict, Marvin L. Cohen, and Steven G. Louie, *Phys. Rev. B* **53**, R13303 (1996); H. Terrones, M. Terrones, E. Hernández, N. Grobert, J-C. Charlier, and P. M. Ajayan, *Phys. Rev. Lett.* **84**, 1716 (2000); X. Rocquefelte, G.-M. Rignanese, V. Meunier, H. Terrones, M. Terrones, and J.-C. Charlier, *Nano Lett.* **4**, 805 (2004).
  - [6] David J. Appelhans, Zhibin Lin, and Mark T. Lusk, *Phys. Rev. B* **82**, 073410 (2010).
  - [7] A. N. Enyashin and A. L. Ivanovskii, *Phys. Status Solidi B* **248**, 1879 (2011).
  - [8] X. L. Sheng, Q. B. Yan, F. Ye, Q. R. Zheng, and G. Su, *Phys. Rev. Lett.* **106**, 155703 (2011).
  - [9] P. B. Sorokin, H. Lee, L. Yu. Antipina, A. K. Singh, B. I. Yakobson, *Nano Lett.* **11**, 2660 (2011).
  - [10] Uwe H. F. Bunz, Yves Rubin and Yoshito Tobe, *Chem. Soc. Rev.* **28**, 107 (1999).
  - [11] M. M. Haley, *Pure Appl. Chem.* **80**, 519 (2008); Joshua M. Kehoe, James H. Kiley, Jamieson J. English, Charles A. Johnson, Ryan C. Petersen, and Michael M. Haley, *Org. Lett.* **2**, 969 (2000).
  - [12] Guoxing Li, Yuliang Li, Huibiao Liu, Yanbing Guo, Yongjun Li and Daoben Zhu, *Chem. Commun.* **46**, 3256 (2010).
  - [13] D. Malko, C. Neiss, F. Viñes, A. Görling, *Phys. Rev. Lett.* **108**, 086804 (2012).
  - [14] Jorge O. Sofo, Ajay S. Chaudhari, and Greg D. Barber, *Phys. Rev. B* **75**, 153401 (2007).
  - [15] D. C. Elias, R. R. Nair, T. M. G. Mohiuddin, S. V. Morozov, P. Blake, M. P. Halsall, A. C. Ferrari, D. W. Boukhvalov, M. I. Katsnelson, A. K. Geim, and K. S. Novoselov, *Science*, **323**, 610 (2009).

- [16] Jayeeta Lahiri, You Lin, Pinar Bozkurt, Ivan I. Oleynik and Matthias Batzill, *Nature Nanotech.* **5**, 326 (2010).
- [17] J. Kotakoski, A. V. Krasheninnikov, U. Kaiser, and J. C. Meyer, *Phys. Rev. Lett.* **106**, 105505 (2011).
- [18] S. W. Slayden and J. F. Liebman, *Chem. Rev.* **101**, 1541 (2001).
- [19] X. Tu, M. A. Zheng, *Nano Res.* **1**, 185 (2008); M. C. Hersam, *Nature Nanotechnol.* **3**, 387 (2008).
- [20] P. Hohenberg and W. Kohn, *Phys. Rev.* **136**, B864 (1964).
- [21] W. Kohn and L. J. Sham, *Phys. Rev.* **140**, A1133 (1965).
- [22] R. Saito, G. Dresselhaus, and M. S. Dresselhaus, *Physical Properties of Carbon Nanotubes* (Imperial College Press, London, 1998).
- [23] G. Kresse, J. Furthmüller, *Phys. Rev. B* **54**, 11169 (1996).
- [24] G. Kresse and D. Joubert, *Phys. Rev. B* **59**, 1758 (1999).
- [25] P. E. Blöchl, *Phys. Rev. B* **50**, 17953 (1994).
- [26] J. P. Perdew, A. Zunger, *Phys. Rev. B* **23**, 5048 (1981).
- [27] J. P. Perdew, Y. Wang, *Phys. Rev. B* **45**, 13244 (1992).
- [28] H. J. Monkhorst, J. D. Pack, *Phys. Rev. B* **13**, 5188 (1976).
- [29] Paolo Giannozzi, Stefano Baroni, Nicola Bonini, Matteo Calandra, Roberto Car, Carlo Cavazzoni, Davide Ceresoli, Guido L Chiarotti, Matteo Cococcioni, Ismaila Dabo, Andrea Dal Corso, Stefano de Gironcoli, Stefano Fabris, Guido Fratesi, Ralph Gebauer, Uwe Gerstmann, Christos Gougoussis, Anton Kokalj, Michele Lazzeri, Layla Martin-Samos, Nicola Marzari, Francesco Mauri, Riccardo Mazzarello, Stefano Paolini, Alfredo Pasquarello, Lorenzo Paulatto, Carlo Sbraccia, Sandro Scandolo, Gabriele Sclauszero, Ari P Seitsonen, Alexander Smogunov, Paolo Umari and Renata M Wentzcovitch, *J. Phys. Condens. Matter* **21**, 395502 (2009).
- [30] Changgu Lee, Xiaoding Wei, Jeffrey W. Kysar and James Hone, *Science* **321**, 385 (2008).
- [31] O. L. Blakslee, D. G. Proctor, E. J. Seldin, G. B. Spence, and T. Weng, *J. Appl. Phys.* **41**, 3373 (1970).
- [32] Y. Baskin and L. Meyer, *Phys. Rev.* **100**, 544 (1955).
- [33] R. A. Andrievski, *Int. J. Refract. Met. Hard Mater.* **19**, 447 (2001).
- [34] S. Reich *et al.*, *Phys. Rev. B* **66**, 035412 (2002).
- [35] T. O. Wehling, K. S. Novoselov, S. V. Morozov, E. E. Vdovin, M. I. Katsnelson, A. K. Geim, and A. I. Lichtenstein, *Nano Lett.* **8**, 173 (2008); M. Deifallah, P. F. McMillan, F. Cora, *J. Phys. Chem. C*, **112**, 5447 (2008); T. B. Martins, R. H. Miwa, Antônio J. R. da Silva, and A. Fazzio, *Phys. Rev. Lett.* **98**, 196803 (2007); F. Cervantes-Sodi, G. Csányi, S. Piscanec, and A. C. Ferrari, *Phys. Rev. B* **77**, 165427



- (2008); Matteo Calandra and Francesco Mauri, *Phys. Rev. B* **76**, 161406(R) (2007); R. Roldán, M. P. López-Sancho, and F. Guinea, *Phys. Rev. B* **77**, 115410 (2008).
- [36] R. Czerw, M. Terrones, J. C. Charlier, X. Blase, B. Foley, R. Kamalakaran, N. Grobert, H. Terrones, D. Tekleab, P. M. Ajayan, W. Blau, M. Rühle, and D. L. Carroll, *Nano Lett.* **1**, 457 (2001); Kai Xiao, Yunqi Liu, Ping'an Hu, Gui Yu, Yanming Sun, and Daoben Zhu, *J. Am. Chem. Soc.* **127**, 8614 (2005).
- [37] P. P. Shinde and V. Kumar, *Phys. Rev. B* **84**, 125401 (2011).
- [38] Yufeng Zhao, Yong-Hyun Kim, A. C. Dillon, M. J. Heben, and S. B. Zhang, *Phys. Rev. Lett.* **94**, 155504 (2005); Mina Yoon, Shenyan Yang, Christian Hicke, Enge Wang, David Geohegan, and Zhenyu Zhang, *Phys. Rev. Lett.* **100**, 206806 (2008); Qiang Sun, Puru Jena, Qian Wang, and Manuel Marquez, *J. Am. Chem. Soc.* **128**, 9741 (2006).
- [39] T. Yildirim and S. Ciraci, *Phys. Rev. Lett.* **94**, 175501 (2005); Hoonkyung Lee, Jisoon Ihm, Marvin L. Cohen, and Steven G. Louie, *Phys. Rev. B* **80**, 115412 (2009).
- [40] C. Ataca, E. Aktürk, and S. Ciraci, *Phys. Rev. B* **79**, 041406(R) (2009).